Low Probability of Interception Radar Signals Detection, Comparison of a YOLOv8 Model and a Conventional Signal Processing Method

Mazouz Reihan, Picheral José, Marcos Sylvie
L2S, CentraleSupelec,
Université Paris-Saclay
2 rue Joliot Curie, 91190 Gif sur Yvette, France
reihan.mazouz@l2s.centralesupelec.fr
jose.picheral@l2s.centralesupelec.fr
sylvie.marcos@l2s.centralesupelec.fr

Taylor Abigael, Bosse Jonathan
DEMR, ONERA,
Universié Paris-Saclay
F-91120 Palaiseau, France
abigael.taylor@onera.fr
jonathan.bosse@onera.fr

***Abstract*—Radar interception plays a critical role in electronic warfare by capturing and analyzing enemy radar emissions. Low Probability of Intercept (LPI) signals are designed to minimize detectability, which poses a significant challenge to conventional detection methods. This paper explores the benefit of the YOLOv8 algorithm, a state-of-the-art deep learning model, for detecting LPI radar signals in time-frequency images. A comparative analysis to assess detection performance is conducted with a common sense solution based on energy detector : the Generalized Likelihood Ratio Test (GLRT). Results demonstrate that YOLOv8 achieves detection with a notable improvement in Peak Signal-to-Noise Ratio (PSNR) for every waveform considered.**

***Index Terms*—Low Probability of Intercept signals, automatic waveform detection, YOLOv8, time frequency analysis, generalized likelihood ratio test**

I. Introduction

Radar interception is a crucial component in the field of electronic warfare, aimed at capturing and analyzing enemy radar emissions for intelligence, jamming, or countermeasure purposes. With technological advancements, radar signals have evolved to become increasingly difficult to detect and intercept, posing significant challenges to current surveillance systems [1].

Low Probability of Intercept (LPI) signals represent a class of radar signals designed to minimize their detection by enemy systems. LPI signal emitters utilize various techniques, the main one being the spreading of energy over time and frequency to reduce the instantaneous power spectral density as much as possible, thereby blending into the ambient noise [1]. Their wide bandwidth and long emission time minimize the energy perceived by the enemy receiver within its acquisition window, thwarting conventional detection mechanisms. Despite the spreading of energy, the matched filter, used particularly by the radar receiver system, maintains the ability to detect the target by recovering the complete signal and correlate with the emitted one [2].

Passive interception methods, on the other hand, do not have prior assumptions about the signal to intecept. To detect, these methods assume certain characteristics such as energy concentration in the time-frequency plane for time-frequency integration methods, a peak in the autocorrelation function for autocorrelation thresholding methods, or signal stationarity for cyclostationary and Quadrature Mirror Filtering detector. Other conventional methods rely on feature extraction, sometimes described as PDW (Pulse Description Words), such as Machine Learning methods or statistical comparison methods to a knowledge database. A description of conventional methods performances for LPI signals detection has been done in [3].

The advent of Deep Learning, however, allows avoiding this constraint of feature extraction and assumptions about key signal characteristics as raw data is processed directly. Its numerous layers can retain key information from data with complex dimensionality. Convolutional Neural Networks (CNNs) are particularly suited for image processing and state of the art presents some CNN based methods for detecting LPI signals [4], [5].

Among CNN architectures, "You Only Look Once" (YOLO) models have revolutionized real-time object detection due to their speed and detection efficiency [6]. State of the art radar interception methods utilize this technology to detect, characterize, and classify waveforms in a time-frequency image [7], [8]. YOLOv8, the eighth version of YOLO, introduces significant improvements in detection performance, especially of objects of various shape dimensions [9], making this technology particularly attractive for application to the detection of LPI radar signals in time-frequency images.

The conventional and deep learning detection chains are depicted in Fig. 1. The ones implemented in this paper are also represented therein.

Although the state of the art includes comparisons of performance between conventional methods and Deep Learning methods for radar target detection [10], to the best of our

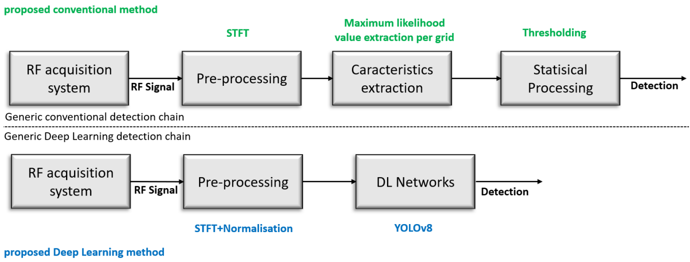

Fig. 1: Block diagram of LPI signal detection using Deep Learning and conventional methods

knowledge, there are no existing comparisons in the literature regarding radar signal interception, particularly for Low Probability of Intercept signals.

The design and adaptation of YOLOv8 for the detection of a wide variety of LPI radar signals and its comparison with a conventional detection algorithm are the main contributions of this publication.

This paper is organized as follows. In Part II, the LPI signals processed and their time-frequency transformation are introduced. In Sections III and IV, YOLOv8 and the selected conventional detection algorithm are presented. The database of signals and the comparison of simulation results are described in Part V. The conclusion is made in Part VI.

II. Signal Models and Pre-processing

The received signal at the interceptor is described by :

$$s(t) = x(t) + n(t) = A \exp\left(2j\pi f_k t + \Phi_k\right) + n(t) \tag{1}$$

It is composed of the signal $x(t)$ emitted by the radar with an amplitude A and the white gaussian noise in the received channel $n(t)$. f_k and Φ_k are the instantaneous frequency and phase, respectively. In this paper, we consider the following LPI waveforms :

- Linear frequency modulations (LFM)
- Non Linear frequency modulations (NLFM)
- Polyphases Codes modulations (P1, P2, P3, P4, Frank, Barker biphasique)
- Costas frequency codes modulations.

All of those waverforms are considered as pulse or as continuous waveforms (CW), and, again, these waveforms are considered LPI when their energy is spread out in time and frequency. However, it would still be possible to detect certain LPI signals in their time-frequency image (TFI) [1].

The TFI of $s(t)$ is obtained by Short Time Fourier Transform (STFT) with a fixed temporal length acquisition window and no overlap. It was shown in [11] that the STFT presents a good compromise in detection problems because it is robust to interferences, computationally efficient, and requires minimal information about the signal's time-frequency characteristics despite the need to carefully select the acquisition window length w. The discrete version is defined as follows:

$$\mathrm{Z}[t_i, f_j] = \sum_{k=1}^{N} s[t_k] \cdot w[t_k - t_i] \cdot e^{-i2\pi k \frac{f_j}{f_s}} \tag{2}$$

The module of the STFT is especially suitable for YOLO algorithms.

III. Structure and Usage of YOLOv8

YOLOv8 is one of the latest versions of the highly popular YOLO architecture achieving notable results in the state-of-the-art LPI détection [7], [8]. This section partially describes the structure of this model which, like its predecessors, mainly consists of three parts: the **Backbone**, the **Neck** and the **Head**.

- The *Backbone* is responsible for extracting features from the input image of fixed size. It uses a series of convolutions and other operations to progressively reduce the spatial dimension of the image while increasing the number of feature channels.
- Through a series of convolutions, upsampling, and concatenations, the *Neck*, derived from [12], connects informations between the different parts extracted from the *Backbone*.
- The *Head* is the final step of detection, taking the outputs features from the *Neck* and using them to predict object classes, bounding boxes, and confidence scores.

An overview of the model architecture is illustrated in Fig. 2.

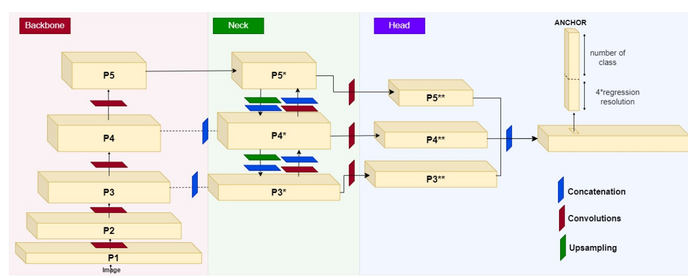

Fig. 2: Overview of the YOLOv8 architecture

A. Anchors in YOLOv8

YOLOv8 is often described as an anchor-free model, however, the concept of anchors is still used in the model's structure, though defined differently from previous object detection models. The last layers of the YOLOv8 Backbone extract features at different resolutions from the initial image which can be depicted as a grid with varying grid sizes. In the model we used, as described in Fig. 2, three layers of the backbone noted as (P3, P4, P5) dividing the image dimension respectively by 16, 32, and 64. Each of these features layer per resolution, named anchor, is used for object detection. The detection and classification cost functions are applied on these anchors during training.

Thus, the anchor structure is responsible for extracting features at different resolution levels in the image, making it valuable for detecting objects of variable dimensions. This functionality therefore presents a significant interest for its use in detecting LPI signals. The dimensions and positions of these signals in the time-frequency image are highly unpredictable, influenced by the parameters of the emitted waveform, the characteristics of the RF reception chain, and the applied time-frequency transform.

B. Usage in Time-Frequency Detection Context

In the proposed approach, we use YOLOv8n (the smallest version of YOLOv8) to detect and localize radar emissions in a time-frequency image. We only retain the coordinates of the bounding boxes, defined by the location and dimension of the predicted object (x_c, y_c, w, h), as well as the confidence score the model attributes to its detection. Thresholding on this score is used to empirically limit the probability of false alarms. An example of bounding boxes is illustrated in Fig 3.

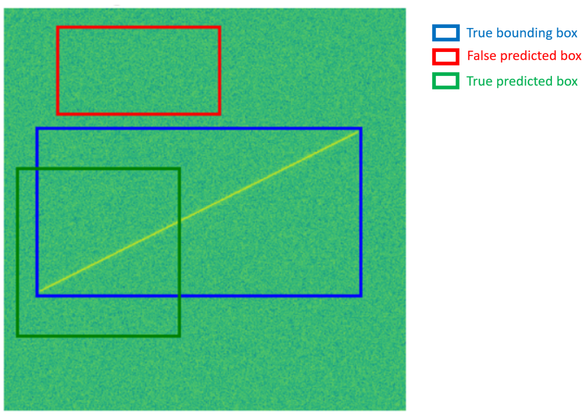

Fig. 3: True and predicted bounding boxes at 10 dB Peak Signal-to-Noise Ratio of a LFM signal

IV. Detector using Generalized Likelihood Ratio Test (GLRT)

To compare the performance achieved by YOLOv8, we have developed a detection algorithm using GLRT on time-frequency image boxes. The assumption behind this detector is that a well chosen group of TFI cells, gathered under a box, can allow detection in low SNR. Especially when the number and proportion of signal cells are high compared to those of pure noise cells. The theoritical background of the GLRT detector is described in the current section.

A. The GLRT Detector

Let $\boldsymbol{Z}$ be a vector composed of N STFT cells, established in (2), following a circular white Gaussian normal complex distribution: $\boldsymbol{Z} \sim \mathbb{C}N(\boldsymbol{M_z}, \boldsymbol{\Gamma})$. $\boldsymbol{M_z}$ is the mean and $\boldsymbol{\Gamma}$ the covariance matrix as defined in [13].

The objective is to ascertain whether a deterministic signal with unknown parameters is present or absent across all points of $\boldsymbol{Z}$ or according to (1), if $s(t) \neq n(t)$.

By applying (2) in (1), $\boldsymbol{M_z}$ is the short time Fourier transform of the noiseless signal $x(t)$, and the following binary hypothesis test is considered:

- H_0: $\boldsymbol{M_z} = \boldsymbol{0_N}$
- H_1: $\boldsymbol{M_z} \neq \boldsymbol{0_N}$

For white Gaussian noise (H_0), the probability density function of $\boldsymbol{Z}$ is:

$$f_0(\boldsymbol{Z}) = \frac{1}{\pi^N |\boldsymbol{\Gamma}|^N} \exp(-\boldsymbol{Z}^* |\boldsymbol{\Gamma}|^{-1} \boldsymbol{Z})$$

And for a signal plus white Gaussian noise (H_1):

$$f_1(\boldsymbol{Z}) = \frac{1}{\pi^N |\boldsymbol{\Gamma}|^N} \exp(-(\boldsymbol{Z} - \boldsymbol{M_z})^* \boldsymbol{\Gamma}^{-1} (\boldsymbol{Z} - \boldsymbol{M_z}))$$

$\boldsymbol{M_z}$ being unkown, we apply the generalized maximum likelihood test to maximize P_D for a fixed P_{FA}. H_1 is selected if the GLRT exceeds a threshold γ :

$$L(\boldsymbol{Z}) = \frac{\max_{\boldsymbol{M_z}} f(\boldsymbol{Z}; H_1)}{f(\boldsymbol{Z}; H_0)} > \gamma$$

In this study we used a non-overlapping window w in (2) to have statistical independance between STFT cells in $\boldsymbol{Z}$. Then $\boldsymbol{\Gamma} = E_w \sigma^2 \boldsymbol{I_N}$, where E_w is the energy of the STFT window w, and σ^2 is the noise variance.

The maximum likelihood for $\boldsymbol{M_z}$ under H_1 is achieved for $\boldsymbol{M_z} = \boldsymbol{Z}$.

Finally:

$$L(\boldsymbol{Z}) > \gamma \iff |\boldsymbol{Z}|^2 > \sqrt{\frac{\log(\gamma) E_w \sigma^2}{N}} = \gamma'$$

For this test, false alarm probability (P_{FA}) and detection probability (P_D) are well known. [14]

Under H_0, $|\boldsymbol{Z}|^2$ follows centered chi-squared distribution with $2N$ degrees of freedom and variance $\frac{\sigma^2}{2N}$.

$$P_{FA} = P(\frac{\gamma'}{\sigma^2}, N) \tag{3}$$

Where P is the regularized gamma function.

Under H_1, $|\boldsymbol{Z}|^2$ follows non centered chi-squared distribution with $2N$ degrees of freedom. P_D is its cumulative density function at γ'.

B. The Grid Detector

In order to stay consistent with our comparison method with the YOLOv8 model, our final detector is a combination of GLRT detections by box on each anchor of the model. The TFI is thus divided by 16, 32 and 64 grids, which we will name G3, G4, G5 (corresponding to P3, P4, P5), and on each of these grids, the GLRT by box is applied. We consider there is a false alarm if there exists a grid whose likelihood ratio exceeds the threshold and which does not intersect with the bounding box of the signal. Conversely, if one of the grids that intersects the bounding box of the signal has its likelihood ratio above the threshold, we consider this to be a detection.

The aggregate probability of False Alarm P_{aFA} across multiple grids is modeled by a binomial distribution, considering each grid as a trial where a false alarm, given in (3), may occur independently. The total probability of at least one false alarm occurring in any of the grids is given by:

$$P_{\mathrm{aFA}} = 1 - \prod_{i=3}^{5} (1 - P_{\mathrm{FA,G}_i})^{N_i} \tag{4}$$

where N_i is the total number of noise grids in G_i and P_{FA,G_i} is the false alarm probability for a single grid of G_i.

The detection probability for the aggregated grids is as follows:

$$P_{\mathrm{aD}} = 1 - \prod_{i=3}^{5} P_{0,\mathrm{G}i}$$

where $P_{0,\mathrm{G}i}$ is the probability that no grid exceeds the threshold:

$$P_{0,\mathrm{G}i} = \prod_{j=0}^{N_i} \left(1 - P_{\mathrm{D,G}_i}(\mu_{j,\mathrm{G}_i}, P_{\mathrm{FA,G}_i})\right)$$

Here, $P_{\mathrm{D,G}i}$, represents the probability of detecting a signal in G_i composed of N_i grids. This probability hinges on the specified false alarm probability, as well as the signal's energy within the grid. This, in turn, is affected by various factors including the waveform, signal power, and the parameters used for the STFT windowing. We will estimate this detection probability numerically.

V. Numerical Experiments

A. Metrics

1) Detection and False Alarm Metrics: In the context of detecting Low Probability of Intercept (LPI) radar signals, the performance evaluation of a detection algorithm relies on the accuracy of predicting bounding boxes and minimizing false alarms. Formally, these criteria are defined as follows:

Let B_r be the actual bounding box of the signal. Let $B_{p,i}$ be the i-th bounding box predicted by the detection algorithm, where $i = 1, 2, ..., N_B$ and N_B represents the total number of predicted bounding boxes.

The condition for a **successful prediction** is given by the existence of at least one non-empty intersection between the true bounding box and one of the predicted bounding boxes:

$$\exists\, B_{p,i} \,:\, B_r \cap B_{p,i} \neq \varnothing$$

Moreover, a **false alarm** is identified for each predicted bounding box that does not meet the condition of intersection with the actual bounding box:

$$\forall\, B_{p,i} \,:\, B_r \cap B_{p,i} = \varnothing$$

A true prediction and a false alarm examples are illustrated in Fig. 3

2) Peak Signal-to-Noise Ratio (PSNR): In the field of image detection, it is common to use the PSNR, which is the ratio between the maximum power reached by the signal and the average power of the noise. In [15], PSNR is used on time frequency images for seismic signals.

The PSNR is written as:

$$PSNR = 10\log_{10}\left(\frac{\max_{f,s} |Z_s(t,f)|^2}{\frac{1}{T_w B_w}\sum_{i=1}^{N_t}\sum_{j=1}^{N_f} |Z_b(t_i,f_j)|^2}\right) \tag{5}$$

where Z_s and Z_b respectively denote a cell of the signal's time-frequency image and a cell of the noise's time-frequency image. N_t and N_f are respectively the number of time samples in the acquisition window and the number of frequency bins in its bandwidth. Unlike SNR, PSNR effectively represents the difficulty to detect and discriminate an LPI waveform. Indeed, a signal spread across time and frequency will be less visible than a short, unmodulated signal at the same SNR.

B. Datasets Experiments

For obvious confidentiality reasons, we do not have access to a real database. Instead, we used a radar simulator to create both our training and testing databases. Both detection algorithms are tested on the same database to evaluate both detection accuracy and false alarm rates.

To best represent the stealth capabilities of LPI radar signals, it is proposed to standardize the diversity of the simulated signals in terms of waveform, PSNR, and dimensions relative to the TFI. To avoid the rescaling steps, each data point has a fixed time-frequency image of dimension 512×512. We have generated a validation database of 1000 data per waveform type, with 100 data per PSNR.

The training database, meanwhile, contains 10000 data per waveform type. The training database considers PSNRs only from 0 dB to 20 dB whereas the testing set considers values from -10 dB to 40 dB. This choice was made because during training, very poor generalization is achieved for PSNRs below 0 dB, significantly increasing the false alarm rate without improving detection probability. For PSNRs above 20 dB, training is simply not necessary. Since our database does not contain any interferences or overlapping signals, we assess the false alarm rate using another database composed of 10 000 pure noise time frequency images.

C. Comparison of Detection Results between the YOLOv8 Model and the Grid Detector

In what follows, we set the same false alarm value for both algorithms by numerical experiments. For the YOLOv8 model we thresholded on the confidence score while we used the theoretical value for the conventional detector.

The false alarm probability has been set to 1×10^{-3} due to limitations in estimating it at lower rates given the size of our noise database. Nevertheless, we still consider this value to be realistic for detecting Low Probability of Intercept (LPI) signals, where false alarm rates tend to be higher than in typical cases. Figure 4 demonstrates the false alarm probability of the YOLOv8 model across associated confidence scores, along with waveform detection probability. The model's confidence in pulse detection varies depending on the waveform class. For a false alarm probability of 1×10^{-3}, the corresponding confidence threshold is 0.28, with no significant reduction in the detection probability for any waveform class.

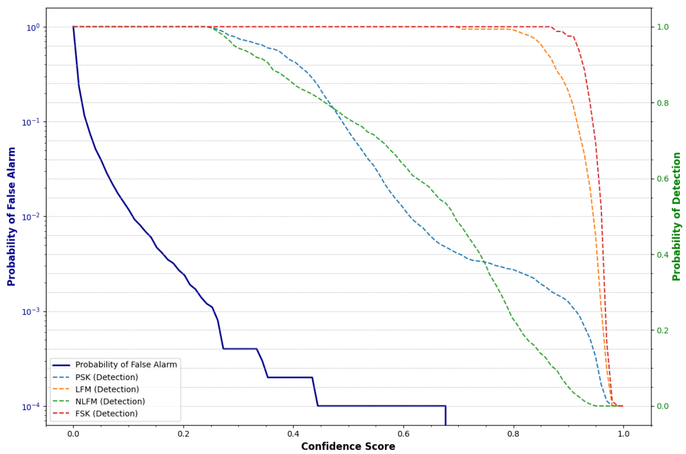

Fig. 4: YOLOv8 Probability of False Alarm (P_{FA}) and Probability of Detection (P_D) per waveforms against confidence threshold

As it can be seen on Fig. 5, the YOLOv8 model is clearly more capable to detect LPI signals at low PSNR. The thresholded PSNR required to achieve a fixed detection probability is reported in Table I for the conventional detector and in Table II for the YOLOv8 detector.

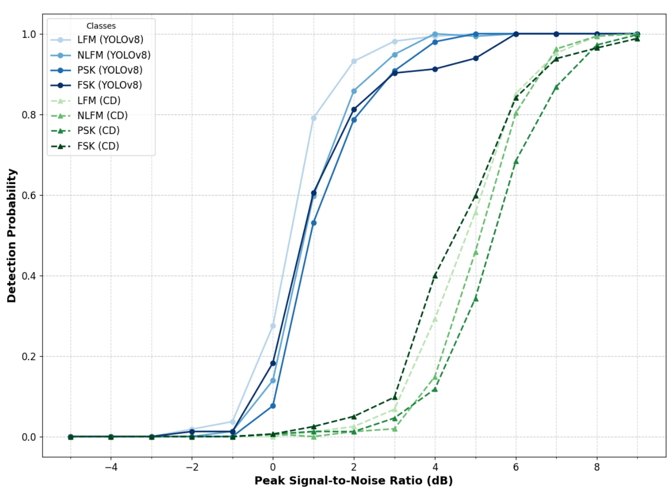

Fig. 5: Probability of detection versus PSNR comparison between Yolov8 in blue and conventional detector (CD) in green

At a constant PSNR, continuous waveforms are slightly better detected than pulses by the conventional detector. However, Yolov8 is not favored when the waveform is continuous, as there is a minimal impact on its detection scores. This observation extends to pulses with high frequency modulation amplitudes as well.

Finally, it is interesting to note that the YOLOv8 model is able to detect most of the pulses at a PSNR of 2 dB for LFM, NLFM, and phase-modulated signals. As it can be seen in Fig.6, at this level of PSNR, a human annotator struggles to distinguish the signals in the time-frequency image and the conventional method often fails.

TABLE I: PSNR (in dB) required for setted probabilities of detection for the conventional detector

		Conventional Detector		
		$P_D 50\%$	$P_D 90\%$	$P_D 99\%$
LFM	Pulse	6	6	9
	CW	5	6	8
NLFM	Pulse	6	7	9
	CW	5	6	8
Phase Shifting	Pulse	6	7	10
	CW	5	6	9
Frequency Shifting	Pulse	5	6	10
	CW	5	6	9

TABLE II: PSNR (in dB) required for setted probabilities of detection for YOLOv8

		YOLOv8		
		$P_D 50\%$	$P_D 90\%$	$P_D 99\%$
LFM	Pulse	0	1	4
	CW	1	1	4
NLFM	Pulse	1	2	4
	CW	1	2	4
Phase Shifting	Pulse	1	2	5
	CW	1	3	5
Frequency Shifting	Pulse	1	2	6
	CW	1	2	6

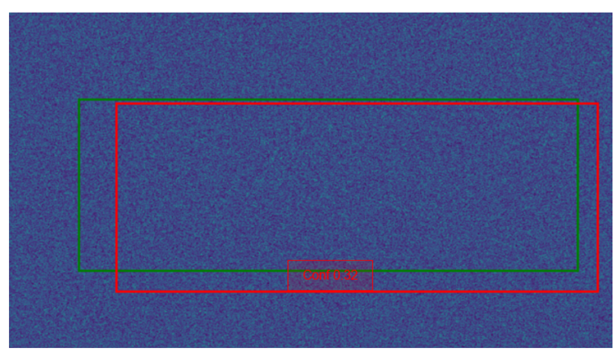

Fig. 6: An illustration of the YOLOv8 detection of a descending chirp for a 2 dB PSNR.

VI. Conclusion

In this paper, a YOLOv8 algorithm for detecting LPI signals in time-frequency images has been trained and tested on various LPI waveforms. Performance has been compared to a conventional GLRT per grid detector at the same False Alarm Probability. For a detection probability of 90%, the

YOLOv8 detector achieves an average gain of 5 dB in Peak Signal-to-Noise Ratio (PSNR) per waveform compared to the conventional detector. All waveforms are detected with almost 100% detection probability at 6 dB of PSNR and with low dispersion between waveforms.

Future work will focus on characterizing the detected signal in addition to detection. The detection cost function of the YOLOv8 model will be adapted to the context of waveform detection in time-frequency images to improve detection qualities and, consequently, characterization.

REFERENCES

[1] P. Pace, Detecting and Classifying Low Probability of Intercept Radar, Second Edition , Artech, 2008.

[2] G. Schrick and R. G. Wiley, "Interception of LPI radar signals," IEEE International Conference on Radar, Arlington, VA, USA, 1990, pp. 108-111.

[3] P. Camuso, G. Foglia and D. Pistoia, "A comprehensive analysis on detection performances of LPI signals filtering strategies," 2009 European Radar Conference (EuRAD), Rome, Italy, 2009, pp. 125-128.

[4] Park, D.-H.; Jeon, M.-W.; Shin, D.-M.; Kim, H.-N. LPI Radar Detection Based on Deep Learning Approach with Periodic Autocorrelation Function. Sensors 2023, 23, 8564.

[5] D. -H. Park, J. -H. Bang, J. -H. Park and H. -N. Kim, "A Fast and Accurate Convolutional Neural Network for LPI Radar Waveform Recognition," 2022 19th European Radar Conference (EuRAD), Milan, Italy, 2022, pp. 89-92.

[6] J. Terven, D. Cordova-Esparza, "A Comprehensive Review of YOLO Architectures in Computer Vision: From YOLOv1 to YOLOv8 and YOLO-NAS" 2023.

[7] S. Sarkar, D. Guo, D. Cabric, "RadYOLOLet: Radar Detection and Parameter Estimation Using YOLO and WaveLet",2023.

[8] D. Reis, J. Kupec, J. Hong, A. Daoudi, "Real-Time Flying Object Detection with YOLOv8",2023.

[9] A. Vagollari, M. Hirschbeck and W. Gerstacker, "An End-to-End Deep Learning Framework for Wideband Signal Recognition," in IEEE Access, vol. 11, pp. 52899-52922, 2023.

[10] D. Brodeski, I. Bilik and R. Giryes, "Deep Radar Detector," 2019 IEEE Radar Conference (RadarConf), Boston, MA, USA, 2019, pp. 1-6.

[11] A. Gupta and A. A. Bazil Rai, "Feature Extraction of Intra-Pulse Modulated LPI Waveforms Using STFT," 2019 4th International Conference on Recent Trends on Electronics, Information, Communication & Technology (RTEICT), Bangalore, India, 2019, pp. 742-746

[12] S. Liu, L. Qi, H. Qin, J. Shi, Jiaya Jia, "Path Aggregation Network for Instance Segmentation", 2018

[13] A. van den Bos, "The multivariate complex normal distribution-a generalization," in IEEE Transactions on Information Theory, vol. 41, no. 2, pp. 537-539, March 1995

[14] H. V. Poor,"An Introduction to Signal Detection and Estimation", chap III,B, p53

[15] Y. Chen, Z. Peng, A. Gholami, J. Yan, S. Li,"Seismic signal sparse time–frequency representation by Lp-quasinorm constraint", Digital Signal Processing, Volume 87, 2019, Pages 43-59, ISSN 1051-2004,